Strojniški vestnik - Journal of Mechanical Engineering vol(yyyy)no, p-p
DOI code
Original Scientific Paper
Received for review: yyyy-mm-dd
Received revised form: yyyy-mm-dd
Accepted for publication: yyyy-mm-dd

Investigation and Optimization of MQL System Parameters in the Roller-Burnishing Process of Hardened Steel

An-Le Van[1] – Trung-Thanh Nguyen[2,*]

[1]Faculty of Engineering and Technology, Nguyen Tat Thanh University, 300A Nguyen Tat Thanh Street, Ward 13, District 4, Ho Chi Minh City 70000, Vietnam

[2]Faculty of Mechanical Engineering, Le Quy Don Technical University, 236 Hoang Quoc Viet, Ha Noi 10000, Vietnam

In the current study, the internal burnishing process under the minimum quantity lubrication (MQL) condition has been optimized to decrease the cylindricity (CYL) and circularity (CIC) of the burnished hole, while the surface roughness (SR) is predefined as a constraint. The optimizing inputs are the diameter of the spray nozzle (D), the spray elevation angle (A), the lubricant quantity (Q), and the pressure value of the compressed air (P). The artificial neural network (ANN) models of burnishing performances are proposed to optimise inputs. The grey relational analysis (GRA) is utilized to compute the weight value of each response. Optimal values of MQL system parameters and technological objectives are selected with the aid of an evolution algorithm (vibration and communication particle swarm optimization (VCPSO) algorithm). The results indicated that the optimal outcomes of the D, A, Q, and P are 1.5 mm, 50 deg, 140 ml/h, and 0.6 MPa, respectively. Furthermore, the CYL, CIC, and SR were decreased by 53.14 %, 57.83 %, and 72.97 %, respectively, at the optimal solution. Finally, the obtained results are expected to be a significant solution to support the machine operator in selecting the optimal MQL system parameters to improve the hole quality in the MQL-assisted burnishing process.
Keywords: internal burnishing; cylindricity; circularity; roughness; ANN; VCPSO

Highlights:

- *Optimization of MQL system parameters, including the diameter of the spray nozzle, spray elevation angle, lubricant quantity, and pressure value of the compressed air.*
- *Consideration of the cylindricity, circularity, and surface roughness.*
- *Development of ANN models for burnishing responses.*
- *Selection of optimal MQL parameters using VCPSO.*

0 INTRODUCTION

The coolant was widely applied to decrease the temperature and friction for different machining operations. However, the massive application of the lubricant increases its cost far higher than the cost of cutting tools, endangers human health, and creates environmental pollution [1]. Manufacturing costs, health, and environmental issues motivate manufacturing enterprises to reduce and eliminate lubricants. Dry machining is the manufacturing operation without the use of any lubricant, which is becoming popular due to environmental safety and worker health [2]. Unfortunately, this method is restricted to the machining of low-strength material with moderate cutting conditions [3] and [4]. An alternative solution is minimum quantity lubrication (MQL), in which a very low amount of fluid (5 ml/h to 200 ml/h) is used in conjunction with compressed air. For different machining of hardened steels and titanium alloys, MQL is a feasible, efficient, and eco-friendly alternative, compared to dry and flood-cooling methods [5].

The MQL method was widely utilized to boost the technical performances of different machining processes. The optimal values of the lubricant quantity (Q), cutting speed (V), and feed rate (f) were selected to decrease the cutting force (CF) of the milling AISI 4140 steel [6]. The specific cutting energy (SCE) model was developed in terms of the V, f, Q, and depth of cut (d) for the MQL end milling process [7]. Moreover, the MQL resulted in 33 % less power consumption (PW) in comparison with the wet approach [8]. Rajan et al. [9] emphasized that the MQL exhibited 157.3 % and 40 % less tool wear (TW) for the turning operation in dry and flood conditions, respectively. Sivaiah et al. [10] revealed that the SR and TW were decreased by

*Corr. Author's Address: Le Quy Don Technical University, 236 Hoang Quoc Viet, Ha Noi, VietNam, trungthanhnguyen@lqdtu.edu.vn

54 % and 7 %, respectively, while the material removal rate (*MRR*) was improved by 27 % for the MQL turning AISI 304. Moreover, the MQL mode could help increase the feed rate by 40 % in the turning EN31 steel [11]. Zhang et al. [12] indicated that the specific grinding energy was significantly decreased using nanoparticle-based MQL. The combination of the MQL and cooled air could be applied to decrease 10.5 % grinding force and 36.3 % roundness errors [13]. A hybrid approach comprising the MQL and water could provide higher cooling-lubrication efficiency [14]. Faverjon et al. [15] stated that the MQL was effectively applied to decrease the thermal distortion and enhance the machined accuracy of the drilled aluminium part. The *SR* and burr height (*BH*) of the drilled hole were significantly reduced under the MQL condition [16]. MQL could be employed to improve the surface morphologies for the drilled composites [17].

The employment of the MQL system in burnishing operations has been rarely addressed in published investigations. The MQL-based diamond-burnishing process was developed and optimized, in which the optimal process parameters, including the spindle speed (*S*), burnishing force (F_b), and *f*, were selected to decrease the *SR* and improve the surface hardness (*SH*) [18]. Similarly, the surface integrity of the burnished titanium alloy was significantly improved using optimal MQL conditions [19]. As a result, missing gaps of the previous publications can be expressed as follows.

The influences of MQL operating parameters, including the nozzle diameter, spray angle, lubricant quantity, and air pressure on geometric errors, have not been analysed in the published investigations. Moreover, predictive models of the cylindricity and circularity regarding the MQL operating parameters for the burnishing operation have not been proposed.

The selection of optimal MQL operating parameters for decreasing geometrical deviations (cylindricity and circularity) and surface roughness for the burnishing operation has not been addressed. The diameter and number of droplets were primarily affected by the lubricant quantity, air pressure, and nozzle diameter, while the machining zone wettability was mainly influenced by the nozzle distance and lubricant quantity [20] and [21]. The spraying angle was related to the workpiece to be machined [22]. Therefore, the optimum setting of MQL system parameters may provide better penetration of the lubricant at the rollers-workpiece interfaces.

Fig. 1. *Burnishing experiment*

1 MATERIAL METHOD

Hardened specimens labelled 5145 are drilled and turned using a computer numerical control (CNC) lathe machine (CTX 400E). The drill tool with a diameter of 16 mm is used to produce the rough hole, in which a feed rate of 0.5 mm/rev, a depth of cut of 8 mm, and a spindle speed of 400 RPM are used as the drilling parameters. Multiple turning paths using polycrystalline cubic boron nitride (CBN) inserts are adopted to turn the internal holes, in which a feed rate of 0.25 mm/rev, a depth of cut of 1 mm, and a spindle speed of 800 RPM are turning factors. The length, internal diameter, and external diameter of each workpiece are 60 mm, 28 mm, and 40 mm, respectively. The cylindricity, circularity, and surface roughness of the pre-machined hole are 70.62 μm, 18.48 μm, and 3.84 μm, respectively.

The burnishing trials are done with the aid of a milling machine, in which the workpiece is positioned and tightly clamped using a jaw-centring chuck (Fig. 1). Soybean oil has been selected as the lubricant and mixed with the compressed air to form the mixture (air-oil mist), which is delivered into the machining region through MQL nozzles. The Mitutoyo Surftest-301 and ZEISS CONTURA G2 are employed to capture the surface roughness, cylindricity, and circularity values.

2 OPTIMIZING FRAMEWORK

The schematic illustration of the internal roller burnishing operation under the MQL condition is depicted in Fig. 2. The MQL system parameters, including the diameter of the spray nozzle, the spray elevation angle, the lubricant quantity, and the pressure value of the compressed air, are presented in Table 1. The ranges of each factor are determined with the aid of the MQL system's characteristics and the manufacturer's recommendations.

The optimization procedure is presented in Fig. 3, which is shown as bellows:

Step 1: The burnishing experiments are executed based on the Box-Behnken design to save the experimental cost [23, 24].

Step 2: The *CYL*, *CIC*, and *SR* models are developed in terms of the MQL system parameters using the ANN approach [25]. The output of the neuron is a function of all inputs and their weights and expressed as [26]:

$$I_j = \sum input_i \times w_{ij}, \quad (1)$$

$$Output_j = f_n(I_j + t_j), \quad (2)$$

where I_j, w_{ij}, t_i, and f_n present the internal value, weight, threshold value, and transfer function, respectively.

The numerical simulations of the ANN model are conducted to calculate the percentage error (PE):

$$PD = \left(\frac{y_a - y_p}{y_a} \right) \times 100, \quad (3)$$

where y_a and y_p are actual and predicted data, respectively. The best architecture of the ANN model with the PE value less than 10 %.

The R^2 value and root mean square error (RMSE) are named as important indicators to investigate the adequacy of the developed models and computed as:

$$R^2 = 1 - \left(\frac{\sum_{i=1}^{n} (y_{pi} - y_{ai})^2}{\sum_{i=1}^{n} (y_{ai})^2} \right), \quad (4)$$

$$RMSE(\%) = \sqrt{\frac{1}{n} \sum_{i=1}^{n} \left(y_{pi} - y_{ai} \right)^2}. \quad (5)$$

Step 3: The weight value of each response is determined using the grey relation analysis (GRA).

The correlation coefficient is calculated as:

$$S_{jl} = \left[\frac{Cov(I_i(j), I_i(l))}{\sigma_{Ii}(j) \times \sigma_{Ii}(l)} \right], \quad (6)$$

where $Cov(I_i(j))$ and $I_i(l)$ presents the covariance of sequences $I_i(j)$ and $I_i(l)$, respectively.

The eigenvalues and consequent eigenvectors are calculated as:

Table 1. *MQL system parameters*

Symbol	Parameters	1	2	3
D	Nozzle diameter [mm]	0.5	1.0	1.5
A	Spray angle [deg]	25	45	65
Q	Lubricant quantity [ml/h]	40	90	140
P	Air pressure [MPa]	0.2	0.4	0.6

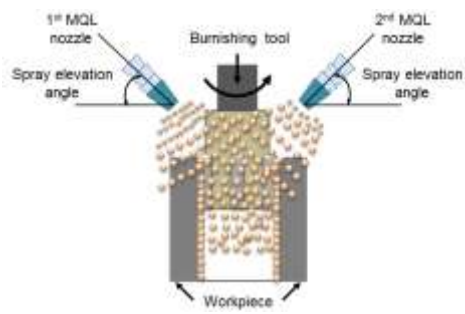

Fig. 2. *The schematic illustration of the internal burnishing operation*

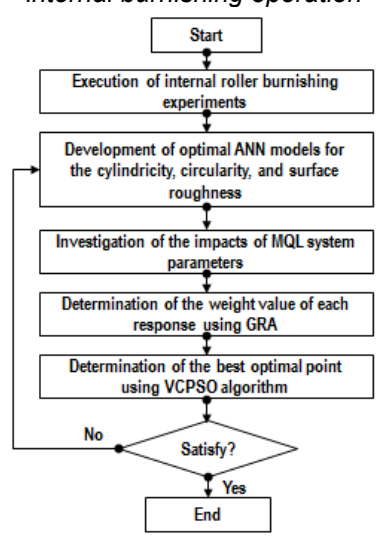

Fig. 3. *The optimization approach for the internal burnishing operation*

$$(S - \lambda_k J_m) V_{ik} = 0, \quad (7)$$

where λ_k, V_{ik}, and J_m presents the eigenvalues, eigenvectors, and the identity matrix, respectively.

The major principal coefficient is calculated as:

$$PC_m = \sum_{i=1}^{n} I_m(i) \times V_{ik}, \quad (8)$$

.

Step 4: The optimal outcomes of the MQL system factors and technical responses are selected using the VCPSO algorithm. Practically, the results produced by the PSO are easily failed into the local optimizing outcomes due to the lack of communication among entire particles. To obtain the global solution, communication with three operations (i.e., the mutation, crossover, and selection) is performed.

The mutation is conducted to exchange information between old and new particles. The mutation operator is expressed as:

$$x_i^{son} = x_{ra} + F(x_{rb} - x_{rc}), \quad (9)$$

where *ra*, *rb*, and *rc* are random integers in the range (0, *N*). The *F* is the scaling factor.

In the crossover stage, the trial vector u_i^{son} is produced to increase the diversity of the population on the basis of the mutation operator. The crossover operation is expressed as:

$$u_{i,d}^{son} = \begin{cases} x_{i,d}^{son} & if\,(rand < CR) \\ x_{i,d}^{son} & otherwise \end{cases}, \quad (10)$$

where *CR* is the crossover rate with the range of (0, 1), d_{rand} is a random number from (1, 2,…, *D*).

The selection operator is enabled to choose better particle between u_i^{son} and x_i using the fitness function, which is expressed as:

$$u_{i,d}^{son} = \begin{cases} x_{i,d}^{son} & if\,(f(u_i^{son}) < f(x_i)) \\ x_{i,d}^{son} & otherwise \end{cases}, \quad (11)$$

.

The equations of the VCPSO algorithm are expressed as follows:

$$v_{id}^{n+1} = \omega v_{id}^{n} + c_1 r_1 (P_{id}^{n} - x_{id}^{n}) + c_2 r_2 (P_{gd}^{n} - x_{id}^{n}) + c_3 r_3 (P_{cd}^{n} - x_{id}^{n}), \quad (12)$$

$$x_{id}^{n+1} = x_{id}^{n} + v_{id}^{n+1}, \quad (13)$$

where c_3 is the accelerated coefficient, while the r_1, r_2 and r_3 are random numbers in range (0, 1), respectively.

3 RESULTS AND DISCUSSIONS

3.1 Development of the Optimal ANN Models

The experimental data of the internal burnishing operation are presented in Table 2, in which the obtained data from experiments No. 1 to 26 are applied to construct the ANN models. The obtained data from experiments No. 27 to 38 are employed to test the accuracy of the developed models. The representative values of the experiments are shown in Fig. 4.

The working parameters of the ANN model are the NT, NN, TF, PM, TS, NL, and LF and their levels are shown in Table 3.

As a result, the training function and the number of hidden neurons have the highest level (14) and the learning function has the minimum level (2). Consequently, the orthogonal array matrix with 256 trials is employed to perform computational trials. The obtained results with the PE values less than 10 % for the ANN model are presented in Table 4. As a result, the optimal outcomes of the NT, NN, TF, PM, TS, NL, and LF are FFNN, TrainLM, 25, MSE, Logsig, 3, and Learn GDM, respectively (the trial No. 146). The PE values of the *CYL*, *CIC*, and *SR* are 3.46 %, 4.21 %, and 3.74 %, respectively. The network with a (4-25-25-25-3) topology has been used for predicting the input-output parameters. The schematic view of the developed ANN model is shown in Fig. 5.

a)

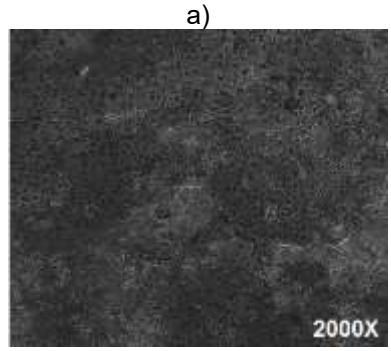

b)

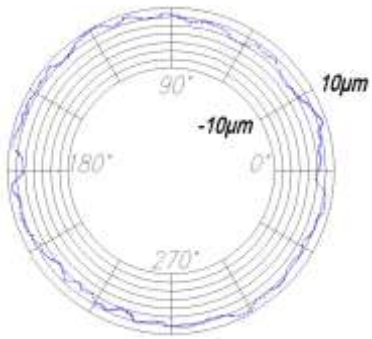

c)

Fig. 4. *Representative results; a) the roughness profile at the No. 21, b) the SEM image of the burnished surface, c) the circularity at the No. 21*

Table 2. *Experimental data for the internal burnishing process*

	No.	*D* [mm]	*A* [deg]	*Q* [ml/h]	*P* [MPa]	*CYL* [µm]	*CIC* [µm]	*SR* [µm]
Experimental data for developing ANN models	1	1.0	65	90	0.2	35.24	14.35	0.42
	2	1.5	65	90	0.4	22.37	10.97	0.34
	3	0.5	25	90	0.4	33.99	17.18	0.52
	4	1.0	25	90	0.2	36.88	15.98	0.48
	5	1.0	65	90	0.6	25.15	9.22	0.27
	6	1.0	25	140	0.4	21.92	11.96	0.29
	7	1.5	45	40	0.4	23.33	12.92	0.41
	8	1.5	45	140	0.4	12.28	6.92	0.21
	9	1.0	25	40	0.4	35.43	18.58	0.51
	10	1.0	25	90	0.6	28.67	12.78	0.32
	11	1.0	45	90	0.4	21.42	9.49	0.38
	12	1.0	45	40	0.2	32.88	14.92	0.53
	13	0.5	65	90	0.4	31.69	14.52	0.44
	14	0.5	45	90	0.6	21.36	10.22	0.35
	15	1.0	65	140	0.4	20.63	9.96	0.23
	16	1.0	45	140	0.2	21.28	9.26	0.28
	17	0.5	45	90	0.2	33.71	13.35	0.51
	18	1.5	25	90	0.4	24.82	12.96	0.38
	19	0.5	45	40	0.4	32.65	16.97	0.54
	20	1.0	65	40	0.4	32.38	16.18	0.45
	21	1.0	45	140	0.6	12.29	5.98	0.14
	22	1.5	45	90	0.6	15.27	5.69	0.16
	23	1.0	45	40	0.6	23.86	12.92	0.36
	24	1.0	45	90	0.4	21.49	9.58	0.37
	25	1.5	45	90	0.2	23.15	10.78	0.39
	26	0.5	45	140	0.4	19.86	9.26	0.38
Experimental data for	27	0.5	40	50	0.5	29.36	15.83	0.53
	28	0.5	40	70	0.4	29.29	14.27	0.51

testing the accuracy of developed ANN models	29	0.5	30	90	0.3	34.12	15.51	0.54
	30	0.5	45	90	0.6	22.31	10.66	0.36
	31	1.0	45	70	0.4	23.82	11.18	0.41
	32	1.0	40	90	0.5	20.45	9.22	0.33
	33	1.0	45	100	0.6	17.66	6.99	0.23
	34	1.0	50	100	0.4	20.43	8.93	0.34
	35	1.5	40	90	0.5	16.84	7.85	0.27
	36	1.5	50	110	0.3	17.59	8.78	0.31
	37	1.5	30	90	0.6	21.11	9.24	0.21
	38	1.5	60	70	0.2	28.52	13.46	0.44

Table 3. *Operating parameters of the ANN models*

Level	Network type (NT)	Number of hidden neurons (NN)	Training function (TF)	Performance function (PM)	Transfer function (TS)	Number of hidden layers (NL)	Learning function (LF)
1	CFNN	15	TrainBFG	MSE	Logsig	1	LearnGDM
2	ELNN	16	TrainBR	MSEREG	Purelin	2	LearnGD
3	FFNN	17	TrainCGB	SSE	Tansig	3	-
4	LRNN	18	TrainCGF	-	-		-
5		19	TrainCGP	-	-		-
6		20	TrainGD	-	-		-
7		21	TrainGDM	-	-		-
8		22	TrainGDA	-	-		-
9		23	TrainGDX	-	-		-
10		24	TrainLM	-	-		-
11		25	TrainOSS	-	-		-
12		26	TrainR	-	-		-
13		27	TrainRP	-	-		-
14		28	TrainSCG	-	-		-

Table 4. *Training results for the developed ANN models*

No.	NT	NN	TF	PM	TS	NL	LF	CYL [%]	CIC [%]	SR [%]
1	CFNN	TrainBFG	16	MSE	Logsig	1	LearnGDM	9.81	8.43	9.46
14	ELNN	TrainOSS	20	MSEREG	Tansig	2	LearnGDM	8.64	7.93	8.78
84	CFNN	TrainLM	26	MSEREG	Tansig	2	LearnGDM	5.71	6.35	5.92
98	CFNN	TrainGDM	28	MSE	Purelin	3	LearnGD	5.43	7.32	5.66
124	LRNN	TrainSCG	18	SSE	Tansig	2	LearnGDM	6.81	7.32	5.81
149	FFNN	TrainLM	25	MSE	Logsig	3	LearnGDM	3.46	4.21	3.74
168	LRNN	TrainGDX	20	MSEREG	Tansig	2	LearnGD	6.38	9.56	6.58
182	ELNN	TrainSCG	22	MSE	Purelin	3	LearnGD	4.44	6.72	4.94
226	ELNN	TrainCGF	28	MSE	Tansig	1	LearnGD	6.74	6.89	6.42

Table 5. *Comparative errors for the burnishing responses*

No.	*CYL* [μm]	*CIC* [μm]	*SR* [μm]

	Exp.	ANN	Err. [%]	Exp.	ANN	Err. [%]	Exp.	ANN	Err. [%]
27	29.36	29.69	-1.12	15.83	15.45	2.40	0.53	0.54	-1.89
28	29.29	28.98	1.06	14.27	14.58	-2.17	0.51	0.52	-1.96
29	34.12	34.53	-1.20	15.51	15.16	2.26	0.54	0.53	1.85
30	22.31	22.68	-1.66	10.66	10.35	2.91	0.36	0.37	-2.78
31	23.82	23.46	1.51	11.18	11.35	-1.52	0.41	0.42	-2.44
32	20.45	20.87	-2.05	9.22	9.39	-1.84	0.33	0.32	3.03
33	17.66	17.24	2.38	6.99	6.88	1.57	0.23	0.22	4.35
34	20.43	20.18	1.22	8.93	8.87	0.67	0.34	0.35	-2.94
35	16.84	16.59	1.48	7.85	7.97	-1.53	0.27	0.26	3.70
36	17.59	17.93	-1.93	8.78	8.61	1.94	0.31	0.32	-3.23
37	21.11	21.54	-2.04	9.24	9.17	0.76	0.21	0.22	-4.76
38	28.52	28.28	0.84	13.46	13.63	-1.26	0.44	0.43	2.27

Exp.: Experimental value; Err.: Error

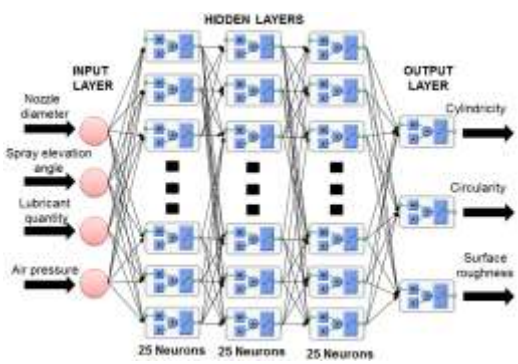

Fig. 5. *The architecture for the ANN models*

The R^2 value and RMSE of the *CYL* model are 0.9652 and 0.0532, respectively. The R^2 value and RMSE of the *CIC* model are 0.9608 and 0.0621, respectively. The R^2 value and RMSE of the *SR* model are 0.9648 and 0.0469, respectively. Therefore, it can be stated that the developed ANN models are adequate and significant.

To investigate the accuracy of the developed ANN model, a set of experiments is performed at random points. The comparisons between the predicted and experimental results are presented in Table 5. The errors of the *CYL*, *CIC*, and *SR* lie within the range of -2.05 % to 2.38 %, -2.17 % to 2.91 %, and -4.76 % to 3.70 %, respectively. The accepted deviations (less than 5.0 %) indicated that the proposed models could be applied to forecast the burnishing performances with good accuracy.

3.2 ANOVA Results for Technological Responses

Table 6 presents ANOVA results for the *CYL* model with significant factors. The computed participations of the *D, A, Q*, and *P* are 15.23 %, 4.12 %, 21.23 %, and 16.52 %, respectively. The computed participations of the *DQ, DP, AQ*, and *AP* are 1.49 %, 3.85 %, 1.57 %, and 1.66 %, respectively. The computed participations of the D^2, A^2, and Q^2 are 24.66 %, 1.76 %, and 7.38 %, respectively.

Table 7 presents ANOVA results for the *CIC* model with significant factors. The computed participations of the *D, A, Q*, and *P* are 11.37 %, 7.64 %, 20.97 %, and 11.69 %, respectively. The computed participations of the *DA, DQ, DP, AP*, and *QP* are 1.11 %, 2.76 %, 3.15 %, 3.11 %, and 2.06 %, respectively. The computed participations of the D^2, A^2, and Q^2 are 4.38 %, 22.78 %, and 7.69 %, respectively.

Table 8 presents ANOVA results for the *SR* model with significant factors. The computed participations of the *D, A, Q*, and *P* are 16.35 %, 6.73 %, 24.81 %, and 19.81 %, respectively. The computed participations of the D^2, A^2, Q^2, and P^2 are 5.38 %, 5.96 %, 3.84 %, and 7.31 %, respectively.

Table 6. *ANOVA results for CYL model*

So.	*SS*	*MS*	*F* value	*P* value
Mo.	1240.283	88.592	21.302	< 0.0001
D	188.895	188.895	45.420	< 0.0001
A	51.100	51.100	12.287	0.0013
Q	262.072	262.072	63.015	< 0.0001
P	204.895	204.895	49.267	< 0.0001
DQ	18.480	18.480	4.444	0.0069
DP	47.751	47.751	11.482	0.0006
AQ	19.472	19.472	4.682	0.0038
AP	20.589	20.589	4.951	0.0024
A^2	305.854	305.854	73.542	< 0.0001
Q^2	21.829	21.829	5.249	0.0021
P^2	91.533	91.533	22.009	0.0003
Res.	49.907	4.159		
Cor.	1288.606			
$R^2 = 0.9652$				
Mo.: Model; So.: Source; Res.: Residual; Cor.: Core total				

Table 7. *ANOVA results for the CIC model*

So.	*SS*	*MS*	*F* value	*P* value
Mo.	302.390	21.599	20.952	< 0.0001
D	34.382	34.382	33.351	< 0.0001
A	23.103	23.103	22.410	< 0.0001
Q	63.411	63.411	61.511	< 0.0001
P	35.349	35.349	34.290	< 0.0001
DA	3.357	3.357	3.256	0.0084
DQ	8.346	8.346	8.096	0.0053
DP	9.525	9.525	9.240	0.0045
AP	9.404	9.404	9.122	0.0046
QP	6.229	6.229	6.043	0.0057
D^2	13.245	13.245	12.848	0.0034
A^2	68.884	68.884	66.820	< 0.0001
Q^2	23.254	23.254	22.557	< 0.0001
Res.	12.337	1.031		
Cor.	314.727			
$R^2 = 0.9608$				

Table 8. *ANOVA results for the SR model*

So.	*SS*	*MS*	*F* value	*P* value
Mo.	0.313	0.022	22.573	< 0.0001
D	0.051	0.051	51.671	< 0.0001
A	0.021	0.021	21.269	0.0003
Q	0.078	0.078	78.407	< 0.0001
P	0.062	0.062	62.605	< 0.0001
D^2	0.017	0.017	17.002	0.0214
A^2	0.019	0.019	18.835	0.0127
Q^2	0.012	0.012	12.135	0.0833
P^2	0.023	0.023	23.102	0.0037
Res.	0.012	0.001		
Cor.	0.324			
$R^2 = 0.9648$				

3.3 Parametric Influences

Fig. 6 indicates that the burnishing responses decrease with increasing nozzle diameter. As the nozzle diameter increases, more droplets can penetrate the burnishing region. The friction at the interfaces decreases, and the cooling-lubrication efficiency increases; hence, low *CYL* and *CIC* values are obtained. Moreover, the burnished surface is efficiently wetted and protected with a higher amount of oil mist; hence, the *SR* decreases.

Fig. 7 presents the impact of the spray elevation angle on the *CYL*, *CIC*, and *SR*, respectively. For the *CYL* and *CIC* values, it can be stated that an increased spray elevation angle has a positive effect, but it turns negative at a certain amount (48 deg), while the turning point of 55 deg is applied for the *SR*. For low spray elevation angle, the penetration of the oil mist is ineffective, resulting in a lack of proper cooling-lubrication efficiency at the interfaces. An uneven deformation is produced along the axial and radial directions; hence, higher values of the *CYL* and *CIC* are obtained. In addition, high friction at the interfaces causes a higher surface roughness. At a higher spray elevation angle, the mist flow is accurately delivered into the machining region, which results in decreased friction; hence, the *CYL* and *CIC* decreases. Higher cooling-lubrication efficiency causes a reduction in surface roughness.

Fig. 8 presents the impact of the *Q* on the *CYL*, *CIC*, and *SR*, respectively. A higher lubricant quantity increases the number of oil droplets entering the contact zone between the roller-workpiece. The cooling-lubrication efficiency will be improved due to friction reduction, which causes uniform deformation; hence, the *CYL* and *CIC* significantly decrease. The burnished surface is wetted and protected due to the penetration of a higher amount of the oil mist; hence, the *SR* decreases.

Figs. 9 indicates that the reductions in the burnishing responses are found with increased air pressure. Higher pressure causes a reduction in the droplet size of the oil mist, while the number of droplets and spraying velocity increase. The small diameter increases the penetration ability into the burnishing region; hence, the cooling-lubrication efficiency is enhanced. The friction between the burnishing tool and workpiece decreases; hence, the burnishing responses reduce.

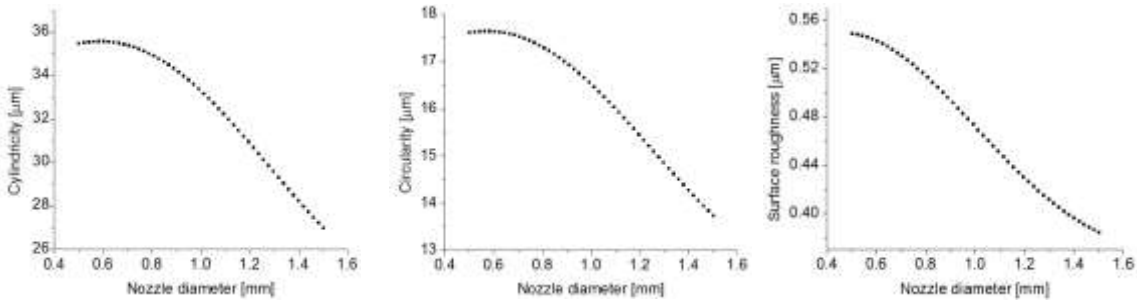

a) b) c)

Fig. 6. *The impacts of the nozzle diameter on the burnishing responses; a) CYL and D, b) CIC and D, c) SR and D*

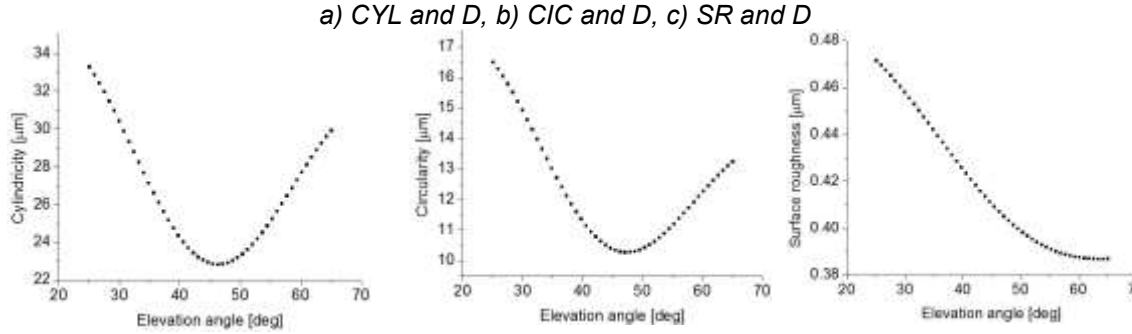

a) b) c)

Fig. 7. *The impacts of the spray elevation angle on the burnishing responses; a) CIC and A, b) CIC and A, c) SR and A*

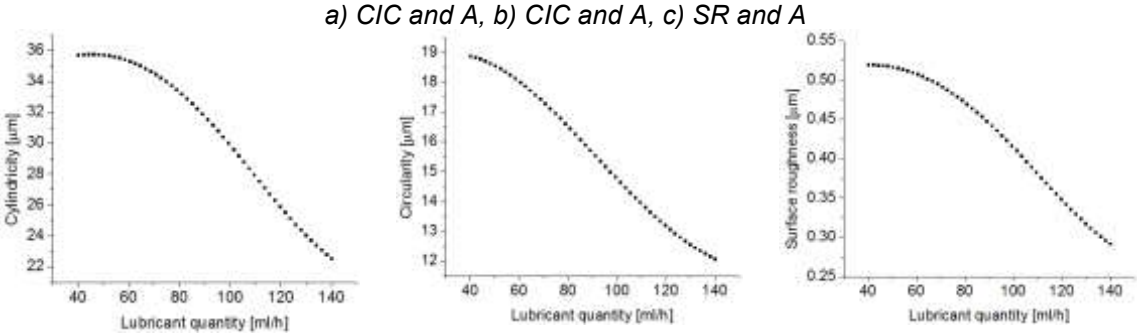

a) b) c)

Fig. 8. *The impacts of the spray elevation angle on the burnishing responses; a) CYL and Q, b) CIC and Q, c) SR and Q*

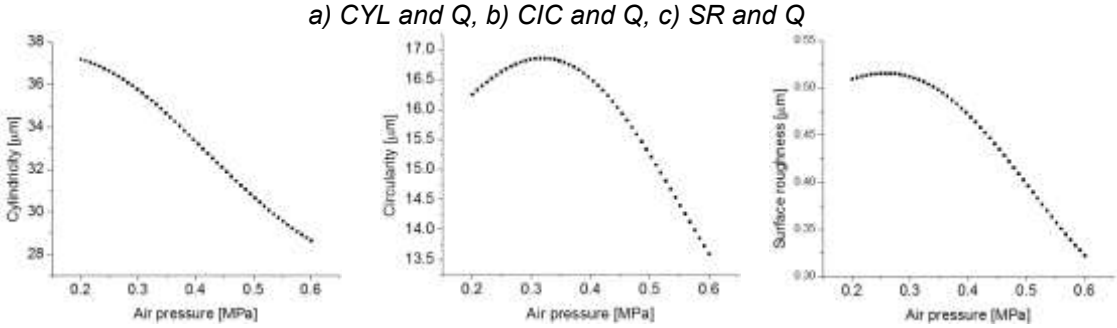

a) b) c)

Fig. 9. *The impacts of the air pressure on the burnishing responses; a) CYL and P, b) CIC and P, c) SR and P*

Table 9. *Optimization results produced by the VCPSO*

Method	*D* [mm]	*A* [deg]	*Q* [ml/h]	*P* [MPa]	*CYL* [μm]	*CIC* [μm]	*SR* [μm]
Initial values	1.0	45	90	0.4	21.49	9.58	0.37
Optimal values	1.5	50	140	0.6	10.07	4.04	0.10
Improvements (%)					53.14	57.83	72.97

3.4 Optimization Results

The proportions of the first principal component is 92.7 %, followed by the second component (4.7 %) and the third component (2.6 %), respectively. The weight values are calculated using the squares of subsequent eigenvectors of the three components. The weight values of the *CYL*, *CIC*, and *SR* are 0.48, 0.34, and 0.18, respectively.

For the high-pressure bushing components, the predefined surface roughness of 0.1 μm is selected. The 3D plot produced with the aid of the VCPSO is shown in Fig. 10. As a result, the optimal values of the *D, A, Q*, and *P* are 1.5 mm, 50 deg, 140 ml/h, and 0.6 MPa, respectively, while the corresponding outcomes of the *CYL*, *CIC*, and *SR* are 10.07 μm, 4.04 μm, and 0.10 μm, respectively (Table 9). The improvements in the *CYL*, *CIC*, and *SR* are 53.14 %, 57.83 %, and 9.64 %, respectively, as compared to the initial values. The *CYL*, *CIC*, and *SR* are decreased by 85.74 %, 78.14 %, and 97.40 %, respectively, as compared to the pre-machined state.

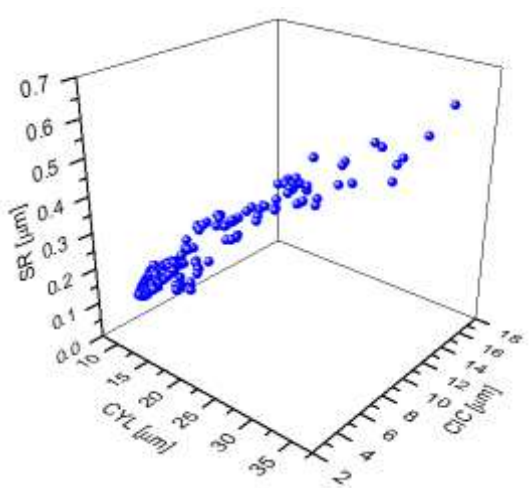

Fig. 10. *3D plots produced by the VCPSO*

4 CONCLUSIONS

In this study, a new MQL-based burnishing process has been proposed and optimized. Instead of traditional process parameters, the inputs considered were MQL operating parameters, including the nozzle diameter, the spray elevation angle, the lubricant quantity, and the pressure value of the compressed air. The quality indicators of the burnished hole, including the cylindricity and circularity, were then addressed and enhanced. The ANN approach was employed to develop the performance models instead of conventional regression models. A new evolutional algorithm entitled VCPSO algorithm was applied to find the optimal solution.

The academic contributions can be expressed as follows:

The proposed optimization technique comprising ANN, GRA, and VCPSO used in this study effectively solves the complex optimizing problems and determines optimal outcomes. The developed approach possesses various advantages, including low experimental costs, decreased human efforts, and easy application by means of Matlab software. The optimizing method can be extensively employed to solve the optimization issues for not only burnishing operations but also other machining processes.

The impacts of the MQL operating parameters (the nozzle diameter, the spray elevation angle, the lubricant quantity, and the pressure value of the compressed air) on the geometric deviations (cylindricity and circularity) and the surface roughness have been thoroughly analysed. The obtained knowledge can help machine operators deeply understand the physical insights in the developed burnishing operation.

The optimized findings can be applied in the burnishing operation to enhance the machining performances. Moreover, the obtained results revealed that the MQL system could be employed to enhance the machining quality of internal holes in various components.

The optimization issues addressing the cylindricity and circularity with a predefined constraint of the surface roughness are realistic

and reliable compared to the simultaneous optimizing three objectives.

The analysed outcomes of the current study can be effectively and efficiently utilized as significant references for future investigations and developing expert systems regarding MQL-assisted internal burnishing processes.

The industrial contributions can be expressed as follows.

In this work, an efficient burnishing operation under the MQL condition has been developed to enhance the machining quality of the internal surface. The successful implementation in the hardened steel is utilized to prove the effectiveness and potential application of the proposed burnishing process. The developed finishing operation can be effectively and efficiently applied to fabricate internal holes.

The constructed ANN models of the *CYL*, *CIC*, and *SR* were significant and accurate. The proposed correlations could be effectively applied to forecast the burnishing responses in industrial applications. The experimental costs and efforts can be saved with the aid of the proposed ANN models.

The 3D plots showing global relationships among machining performances can support machine operators in selecting the optimal values of the MQL operating factors, circularity, and cylindricity under various constraints of the surface roughness for different purposes.

The influences of the MQL system parameters on energy consumption and production costs have not been presented. A comprehensive optimization considering more objectives will be explored in future works.

5 ACKNOWLEDGEMENTS

This research is funded by Vietnam National Foundation for Science and Technology Development (NAFOSTED) under grant number 107.04-2020.02.

6 REFERENCES

[1] Khan, M.M.A., Mithu, M.A.H., Dhar, N.R. (2009). Effects of minimum quantity lubrication on turning AISI 9310 alloy steel using vegetable oil-based cutting fluid. *Journal of Materials Processing Technology*, vol. 209, no.15-16, p. 5573-5583, DOI:10.1016/j.jmatprotec.2009.05.014.

[2] Kỳvak, T., Şeker, U. (2015). Effect of cryogenic treatment applied to M42 HSS drills on the machinability of Ti–6Al–4V alloy. *Materials and Technology*, vol. 49, no. 6, p. 949-956, DOI:10.17222 /mit.2014.283.

[3] Goindi, G.S., Sarkar, P. (2017). Dry machining: a step towards sustainable machining-challenges and future directions. *Journal of Cleaner Production*, vol. 165, p. 1557-1571, DOI:10.1016/j.jclep ro.2017.07.235.

[4] Maruda, R.W., Krolczyk, G.M., Wojciechowski, S., Powalka, B. Klos, S., Szczotkarz, N. Matuszak, M. Khanna, M. (2020). Evaluation of turning with different cooling-lubricating techniques in terms of surface integrity and tribologic properties. *Tribology International*, vol. 148, art. ID, 106334, DOI:10.1016/j.triboint.2020.10633.

[5] Szczotkarz, N., Mrugalski, R., Maruda, R.W., Królczyk, G.M., Legutko, S., Leksycki, K. Dębowski, D., Pruncu, C.I.g(2021). Cutting tool wear in turning 316L stainless steel in the conditions of minimized lubrication. *Tribology International*, vol. 156, art. ID 106813, DOI:10.1016/j.triboint.2020.10681.

[6] Mia, M., Bashir, M.A., Khan, M.A., Dhar, N.R. (2017). Optimization of MQL flow rate for minimum cutting force and surface roughness in end milling of hardened steel (HRC 40). *The International Journal of Advanced Manufacturing Technology*, vol. 89, p. 675-690, DOI:10.1007/s00170-016-9080-8.

[7] Jang, D., Jung, J., Seok, J. (2016). Modeling and parameter optimization for cutting energy reduction in MQL milling process. *International Journal of Precision Engineering and Manufacturing-Green Technology*, vol. 3, p. 5-12, DOI:10.1007/s40684-016-0001-y.

[8] Bayat, M., Abootorabi, M.M. (2021). Comparison of minimum quantity lubrication and wet milling based on energy consumption modeling. *Proceedings of the Institution of Mechanical Engineers, Part E: Journal of Process Mechanical Engineering*, vol. 235, no. 5, p. 1665-1675, DOI:10.1177/09544089211014407.

[9] Rajan, K.M., Kumar Sahoo, A., Chandra Routara, B., Kumar, R. (2021). Investigation on surface roughness, tool wear and cutting power in mql turning of bio-medical Ti-6Al-4V ELI alloy with sustainability. *Proceedings of the Institution of Mechanical Engineers, Part E: Journal of Process Mechanical Engineering,* DOI:10.1177/09544089211063712.

[10] Sivaiah, P., Venkata Ajay kumar, G,, Lakshmi Narasimhamu, Balaji, N.S. (2021). Performance improvement of turning operation during

processing of AISI 304 with novel textured tools under minimum quantity lubrication using hybrid optimization technique. *Materials and Manufacturing Processes*, DOI:10.1080/10426914.2021.1967977.

[11] Bhadoria, N.S., Bartarya, G. (2021). On the improvement in process performance of ceramic inserts during hard turning in MQL environment. *Materials and Manufacturing Processes*, vol. 37, no. 3, p. 283-293, DOI:10.1080/10426914.2021.1967978.

[12] Zhang, D., Li, C., Zhang, Y., Jia, D, Zhang, X. (2015). Experimental research on the energy ratio coefficient and specific grinding energy in nanoparticle jet MQL grinding. *The International Journal of Advanced Manufacturing Technology*, vol. 78, p. 1275-1288, DOI:10.1007/s00170-014-6722-6.

[13] Ribeiro, F.S.F., Lopes, J.C., Garcia, M.V., de Moraes, D.L., da Silva, A.E., de Angelo Sanchez, L.E., de Aguiar, P.R., Bianchi, E.C. (2020). New knowledge about grinding using MQL simultaneous to cooled air and MQL combined to wheel cleaning jet technique. *The International Journal of Advanced Manufacturing Technology*, vol. 109, p. 905-917, DOI: 10.1007/s00170-020-05721-z.

[14] De Moraes, D.L., Garcia, M.V., Lopes, J.C., Fonteque Ribeiro, F.S., de Angelo Sanchez, L.E., Foschini, C.R., de Mello, H.J., Aguiar, P.R., Bianchi; E.C. (2019). Performance of SAE 52100 steel grinding using MQL technique with pure and diluted oil. *The International Journal of Advanced Manufacturing Technology*, vol. 105, p. 4211-4223, DOI:10.1007/s00170-019-04582-5.

[15] Faverjon, P., Rech, J., Valiorgue, F., Orset, M. (2015). Optimization of a drilling sequence under MQL to minimize the thermal distortion of a complex aluminum part. *Production Engineering*, vol. 9, p. 505-515, DOI:10.1007/s11740-015-0614-y.

[16] Chakravarthy, V.V.K., Rajmohan, T., Vijayan, D., Palanikumar, K. (2021). Sustainable drilling of Nano sic reinforced al matrix composites using MQL and cryogenic cooling for achieving the better surface integrity. *Silicon,* .vol. 14, p. 1787-1805, DOI:10.1007/s12633-021-00977-w.

[17] Xu, J., Ji, M., Chen, M., Ren, F. (2019). Investigation of minimum quantity lubrication effects in drilling CFRP/Ti6Al4V stacks. *Materials and Manufacturing Processes*, vol. 34, p. 1401-1410, DOI:10.1080/10426914.2019.1661431.

[18] Sachin, B., Narendranath, S., Chakradhar, D. (2019). Selection of optimal process parameters in sustainable diamond burnishing of 17-4 PH stainless steel. *Journal of the Brazilian Society of Mechanical Sciences and Engineering*, vol. 41, p. 219, DOI:10.1007/s40430-019-1726-7.

[19] Sachin, B., Narendranath, S., Chakradhar, D. (2019). Effect of working parameters on the surface integrity in cryogenic diamond burnishing of 17-4 PH stainless steel with a novel diamond burnishing tool. *Journal of Manufacturing Processes*, vol. 38, p. 564-571, DOI:10.1016/j.jmapro.2019.01.051.

[20] Maruda, R.W., Krolczyk, G.M., Feldshtein, E., Pusavec, F., Szydlowski, M., Legutko, S., Sobczak-Kupiec, A. (2016). A study on droplets sizes, their distribution and heat exchange for minimum quantity cooling lubrication (MQCL). *International Journal of Machine Tools and Manufacture*, vol. 100, p. 81-92, DOI:10.1016/j.ijmachtools.2015.10.

[21] Maruda, R.W., Feldshtein, E., Legutko, S., Krolczyk, G.M. (2016). Analysis of contact phenomena and heat exchange in the cutting zone under minimum quantity cooling lubrication conditions. *Arabian Journal for Science and Engineering*, vol. 41, p. 661-668, DOI 10.1007/s13369-015-1726-6.

[22] Maruda, R.W., Feldshtein, E., Legutko, S., Krolczyk, G.M. (2015). Research on emulsion mist generation in the conditions of minimum quantity cooling lubrication (MQCL). *Technical Gazette - Tehnicki Vjesnik*, vol. 22, no. 5, p. 213-1218 DOI:10.17559/TV-20140423221850.

[23] Sampath, B., Myilsamy, S. (2021). Experimental investigation of a cryogenically cooled oxygenmist near-dry wire-cut electrical discharge machining process. *Strojniški vestnik - Journal of Mechanical Engineering*, vol. 67, no. 6, p. 322-330, DOI:10.5545/sv-jme.2021.7161.

[24] Nguyen, T.T., Le, T.M. (2021). Optimization of the internal roller burnishing process for energy reduction and surface properties. *Strojniški vestnik - Journal of Mechanical Engineering*, vol. 67, no. 4, p. 167-179, DOI:10.5545/sv-jme.2021.7106.

[25] Milčić, D., Alsammarraie, A., Madić, M., Krstić, V., Milčić, M. (2021). Predictions of friction coefficient in hydrodynamic journal bearing using artificial neural networks. *Strojniški vestnik - Journal of Mechanical Engineering,* vol. 67, no. 9, p. 411-420, DOI:10.5545/sv-jme.2021.7230.

[26] Rosel Solís, M., Dávalos Ramírez, J., Molina Salazar, J., Ruiz Ochoa, J., Gómez Roa, A. (2021). Optimization of running blade prosthetics utilizing crow search algorithm assisted by artificial neural networks. *Strojniški vestnik - Journal of Mechanical Engineering*, vol. 67, no. 3, p. 88-100. DOI:10.5545/sv-jme.2020.6990.